Journal of Nuclear Materials 447 (2014) 38–45

Contents lists available at ScienceDirect

Journal of Nuclear Materials

journal homepage: www.elsevier.com/locate/jnucmat

Recovery of actinides from actinide–aluminium alloys by chlorination: Part II

P. Souček [a],*, L. Cassayre [b], R. Eloirdi [a], R. Malmbeck [a], R. Meier [a], C. Nourry [a], B. Claux [a], J.-P. Glatz [a]

[a] *European Commission, JRC, Institute for Transuranium Elements, Postfach 2340, 76125 Karlsruhe, Germany*

[b] *Laboratoire de Génie Chimique (LGC), Département Procédés Electrochimiques, CNRS-UMR 5503, Université de Toulouse III – Paul Sabatier, 31062 Toulouse Cedex 9, France*

ARTICLE INFO

Article history:
Received 24 September 2013
Accepted 11 December 2013
Available online 18 December 2013

ABSTRACT

A chlorination route is being investigated for recovery of actinides from actinide–aluminium alloys, which originate from pyrochemical recovery of actinides from spent metallic nuclear fuel by electrochemical methods in molten LiCl–KCl. In the present work, the most important steps of this route were experimentally tested using U–Pu–Al alloy prepared by electrodeposition of U and Pu on solid aluminium plate electrodes. The investigated processes were vacuum distillation for removal of the salt adhered on the electrode, chlorination of the alloy by chlorine gas and sublimation of the $AlCl_3$ formed. The processes parameters were set on the base of a previous thermochemical study and an experimental work using pure UAl_3 alloy. The present experimental results indicated high efficiency of salt distillation and chlorination steps, while the sublimation step should be further optimised.

1. Introduction

A chlorination route is under investigation at ITU for recovery of actinides (An) from actinide–aluminium (An–Al) alloys, which originate from pyrochemical treatment of spent metallic nuclear fuel by electrochemical methods in molten LiCl–KCl [1,2]. The background, principles and thermodynamic calculation related to the method have been described in detail in the previous work [3]. The present work was focused on a laboratory-scale demonstration of the process using U–Pu–Al alloy prepared by electrodeposition of U and Pu on solid aluminium plate electrodes by electrorefining of U–Pu–Zr alloy in the molten salt. All the most important steps of the chlorination route were tested, i.e., vacuum distillation for removal of the salt adhered on the electrode, chlorination of the alloy by chlorine gas and sublimation of the $AlCl_3$ formed. The tested experimental conditions were derived from the previous thermochemical study on the process and from the chlorination experiments with UAl_3 alloy [3]. The conditions were set to provide complete chlorination, but preventing volatilisation of the present actinides. All the process steps were evaluated on the basis of X-ray diffraction (XRD) analyses of the reacting material, combined in some cases with inductively-coupled plasma mass spectrometry (ICP-MS) or optical emission spectrometry (ICP-OES) and scanning electron microscopy coupled with energy-dispersive X-ray spectroscopy (SEM-EDX) measurements.

2. Preparation of U–Pu–Al alloys

The initial material was prepared by potentiostatic electrorefining of U–Pu–Zr alloy (71–19–10 wt.%, respectively, ITU stock material) in LiCl–KCl eutectic melt (Aldrich 99.99%) using Al plate cathodes (99.999%, Alfa Aesar). Three runs were carried out at a temperature of 450 °C, yielding alloys with different actinide content due to development of actinides concentrations in the melt. A detailed description of the electrorefining process can be found elsewhere [4].

2.1. Experimental – electrorefining

The electrorefining runs were carried out in a glovebox under purified Ar atmosphere (<5 ppm of moisture and oxygen). The electrolyte consisted of LiCl–KCl eutectic melt containing UCl_3 and $PuCl_3$ (1.78 and 0.62 wt.% metal, respectively) was prepared by chemical oxidation of the U–Pu–Zr alloy by $BiCl_3$ according to the procedure described in [5]. The formed Bi metal was collected in a Bi pool at the bottom of an alumina crucible. After the reaction was completed, which was evidenced by electrochemical measurement, the melt was slowly cooled to solid state, the crucible was broken and the Bi pool was mechanically removed. The recovered melt was transferred to a new alumina crucible and used as the electrolyte. The U–Pu–Zr alloy was loaded in a Ta basket and connected as an anode. Cathodes were made of Al plates with dimensions of the immersed parts 10 × 10 × 0.5 mm. The reference electrode used was an Ag/LiCl–KCl–AgCl (1 wt.%) prepared in a Pyrex glass tube. PAR 273 potentiostat with EG&G

---

* Corresponding author. Tel.: +49 7247951124.
E-mail address: pavel.soucek@ec.europa.eu (P. Souček).

0022-3115/$ - see front matter © 2013 Elsevier B.V. All rights reserved.
http://dx.doi.org/10.1016/j.jnucmat.2013.12.011

M270 electrochemical software was used to control the electrorefining.

2.2. Electrorefining runs

A potential of −1.30 V vs. Ag/AgCl, which is suitable for deposition of both actinides on solid aluminium [6,7], was used for all electrorefining runs. The value of passed charge was selected in a way to produce deposits using approximately 70–80% of Al plates capacity, assuming current efficiency 80% and formation of $AnAl_3$ alloys. Typically, the current density decreased during the runs from −15 to −6 mA/cm^2 due to the slowing down of intermetallic diffusion of An and Al through the An–Al alloy formed on the electrode surface. The development of current in dependency on the passed charge is shown in Fig. 1 for a partly exceptional case in run 2. The initial current decrease was followed by a stable current and in the final phase even increasing current. It can be explained by co-deposition of Zr dissolved from the anode at the later stage of this run, as the deposition potential of Zr is approximately 250 mV more positive than for U, which could yield higher deposition rate and consequently the increasing current. Another explanation can be based on the increase of the surface area in this run due to a different morphology of Zr containing deposit, but this feature was not observed in this particular case, when only 0.6 wt.% of Zr was co-deposited.

The concentration profile, shown in Fig. 2 (left), indicates an increasing concentration of Pu in the electrolyte. U and Pu are congruently electrochemically dissolved from the U–Pu–Zr alloy [8], but U is electrodeposited predominantly on Al due to its more anodic deposition potential in comparison with Pu [6,7]. It led to higher consumption of U from the electrolyte, i.e., decreasing of U concentration and increase of Pu concentration. The U concentration increase observed after run 1 is probably not correct due to possible cross contamination of the ICP-MS sample during preparation in U contaminated glove boxes.

Due to substantially more positive electrode potential of Zr electrochemical oxidation than these of U and Pu, Zr is generally not dissolved in the melt until major part of the actinides are removed from the U–Pu–Zr alloy [8]. During runs 1 and 2 (Fig. 2_right) about 70 wt.% of U and Pu was removed from the initial alloy and it finally led to partial co-dissolution of Zr to the melt. Before run 3, a new pin of the U–Pu–Zr alloy was thus added to the anode basket to reduce the Zr content in the melt and to provide conditions for more efficient preparation of the last required An–Al alloy deposit. The ICP-MS results confirmed full reduction of the dissolved Zr, however they also showed an unexpected decrease of U and Pu concentration in the melt (Fig. 2_left). It indicates relatively high uncertainty of the ICP-MS in this case, nevertheless the general trends in the concentration developments are well illustrated by these results. The expected development of anodic material composition during the runs is shown in Fig. 2 (right).

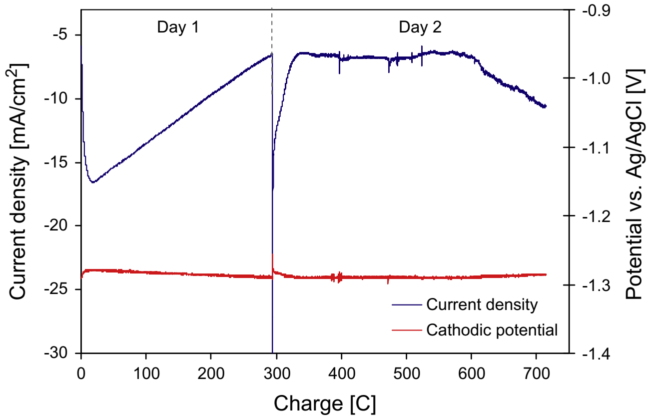

Fig. 1. Development of current density (upper line) with the passed charge during electrochemical preparation of U–Pu–Al alloy, run 2.

2.3. Material characterisation

After the required charge was passed, each electrode was left above the melt surface for several hours at working temperature to let some adhered salt drop off the surface. In all cases, shiny metallic-looking deposit was obtained, homogeneously distributed and well adhered on the electrode surface. A cross section of the electrode with the deposit from run 2 is shown in Fig. 3a.

The deposit was mechanically scraped without washing, homogenised by fine grinding in a mortar and sampled for XRD and ICP-MS analyses.

The mass balance of the electrodeposition runs based on ICP-MS results is summarised in Table 1. The masses of An in the deposits were corrected from the evaluated An content in the adhered salt. To illustrate the achieved capacity of Al to take up actinides, a loading of each electrode was calculated using a mass ratio of the deposited An and the immersed part of Al electrode. The maximum possible An/Al ratio was derived from the alloy composition $An–Al_3$, typically formed during the electrorefining process [5].

Consistently with the concentration profiles presented in Fig. 2, the increasing content of Pu in the product along the three runs was caused by its increasing concentration in the salt. Since the equilibrium potential (E_{eq}) is concentration dependent according to Nernst law, at the later stage of the process, the overvoltage between E_{eq} and the deposition potential E_{dep}, is increasing. Therefore, according to Butler–Volmer equation, higher portion of Pu was co-deposited with U.

Somewhat lower current efficiency achieved in run 2 might be explained by co-deposition of Zr on the Al cathode. A deterioration of An–Al deposits macroscopic structure and lowering of current efficiency has been positively observed in previous electrorefining experiments for the cases of Zr co-dissolution and co-deposition [5]. A higher salt content detected in the corresponding deposit by ICP-MS and also the highest mass loss of the material during distillation supports this explanation (see Section 3.3.1 below); however no worsening of the deposit macroscopic quality was observed.

The X-ray diffraction analyses have been performed on a Bruker D8 Bragg-Brentano Advance diffractometer (Cu Kα1 radiation) equipped with a Lynxeye Linear Position Sensitive detector. The operation conditions were 40 kV and 40 mA. Powder diffraction patterns were recorded at room temperature across an angular range $10° \leqslant 2\theta \leqslant 120°$. The phase quantification procedure involved in the identification of the different phases was done using the software Match (Crystal Impact) and quantification of phases of all data sets was done by the full profile Rietveld method implemented in the software Topas version 4.1. (Coelho, 2007). The starting structure models were adopted from the Inorganic Crystal Structure Data Base (ICSD). The computations involved adjustment of the scale factors, pattern background polynomial parameters, the sample displacement, lattice parameters and peak profile options. The refinement of preferred orientation was done by the March–Dollase Model with an order of 4–8. Depending on the analyses conditions, scan time and sample preparation, the detection limit of X-ray diffraction can be of the order of 1–5 wt.%. Due to close crystallographic parameters of UAl_x and $PuAl_x$ or a solid solution of both phases, XRD cannot distinguish them, as the differences in the positions of the corresponding diffraction peaks are below resolution of the instrument. The same is valid for chlorides UCl_3 and $PuCl_3$. To determine the U/Pu ratio and to extend the